Main influence factors on the physical drying of printing inks with regard to drying systems

Scheuter, Karl R.; Dosdoğru, G.

(1969)

10 th International Conference of Printing Research Institutes

Vienna 1969

Main influence factors on the physical drying of printing inks with regard to drying systems

K. R. Scheuter · G. Dosdoğru

Institut für Druckmaschinen und Druckverfahren

der Technischen Hochschule Darmstadt

Institutsdirektor: o. Prof. Dipl.-Ing. Karl R. Scheuter

Mai 1969

69/1

Xth International Conference of IARIGAI in Vienna June 1969

Main Influence Factors on the Physical Drying of Printing Inks with Regard to Drying Systems.

The drying of printing inks either comes about mainly by chemical or mainly by physical changes in the ink film applied. In the following, we will discuss only the physical drying, since the engineer can only influence this type of drying with respect to a dryer optimization, by allowing for mathematical interrelations and by suitable designs. Printing ink, consisting of resins, pigments, solvents, etc., represents a very complex material to be dried. Nevertheless, it has during physical drying two processes in common with all other materials to be dried: firstly, the transition of liquid into vaporous state and secondly, the carrying off of the vapor that forms.

Independent of the type of heat input, we may state as a rule with regard to economy and the careful handling of material to be dried, that if possible, only so much heat should be supplied as can be carried away by the released vapor. This rule should be particularly observed when designing a dryer for printing presses, since the material to be imprinted because of such known difficulties as register inaccuracies for example, should be heated as little as possible.

The drying theory, which describes the coupling between heat and vapor transfer allows us to derive mathematical interrelations in first approximation for printing inks also. For over 100 years, theoretical and experimental studies of a great many different materials to be dried were made in cases where the location of the vapor formation was the surface of the wet material. It is, therefore, possible by observing the similarity laws, to apply these studies within limits to a liquid ink film.

In the following, some results of theoretical examinations of Toluene evaporation will be related, which were attained with the aid of an extensive computer program. We will, however, refrain from discussing the theory within this report. A brief explanation of the assumption upon which the computations were based, shall, however, be given. For the computations a complete

liquid Toluene layer was presupposed. Furthermore, knowledge of all material data for liquid and vaporous Toluene in dependency on temperature was required. These data were collected as far as they were available from international tabular compilations. Some of the unknown data at certain temperatures were determined by interpolation.

It is known, that the heat and mass transfer takes place in the boundary layer of the surface of a liquid. It is also known, that with greater concentration in this boundary layer not only the data of the carrier gas - in this case air - play a decisive role in the heat and mass transfer, but also the data for the Toluene-air mixture. Neglecting this fact in theoretical computations leads to erroneous results. For this reason, the computations for the Toluene-air mixture were based on the material data determined in accordance with the known mixing laws for gasses. Their computation requires lengthy iterations which can only be carried out with the help of a computer. For all other computations air was considered the heat carrier.

First of all it was necessary to determine the surface temperature created on the surface of the liquid Toluene at a given air temperature. The result from these computations may be seen in fig. 1. There the air temperature t_L is plotted in dependency on the surface temperature t_w. The partial pressure of the Toluene vapor P_{DL} in the air is hereby the variable parameter. It may be seen that at a given air temperature with an increase of the partial pressure, - i.e. with higher vapor concentrations - the surface temperature also rises.

First of all, the problem shall be discussed of how the drying rate in kg/m^2h changes at free convection with an increase in surface temperature. The type of heat input is of subordinate importance for this consideration. Fig. 2 shows the results of the computation. The curve is valid for a circular drying area with a diameter of D = 2m. With an increase of the surface temperature, the drying rate increases considerably. At a surface temperature of 110° C which corresponds to the boiling point of Toluene, a drying rate of approximately 28 kg/m^2h is reached. For various reasons, such a high temperature of the Toluene layer, which corresponds approximately to the temperature on the surface of a material to be imprinted, may never be reached. In rotogravure printing the temperature of the material to be imprinted should, if at all possible, not

exceed 40 - 45° C. In this case, at free convection a very low drying rate would be attained. An increase of the drying rate is only possible by increasing the vapor movement by additional movement of the carrier gas. How this additional movement, namely the forced convection, influences the drying rate at a given surface temperature, is shown in fig. 3. It represents the dependency of the drying rates on the average air velocity along the surface and on the surface temperature. In order to be able to compare the drying rates with the values determined in Fig. 2, a circular area with a diameter D = 2 m was likewise selected.

For the computation it is necessary to know the condition of flow besides the relationship between surface and air temperatures given in fig. 1. We know that there are various types of flow, as for example tangential flows or multiple or single impinging jet arrangements. These types of flows have been more or less intensively discussed in pertinent literature. Particularly the single circular impinging jet is well known, e.g. Schrader [1]; Schlünder und Gnielinski [2]; Petzold [3]; Perry [4]. For this reason, the single circular impinging jet was used as a basis for the computations.

Fig. 3 allows us to make some statements which are of great importance for evaluation of drying systems. At average air velocities along the surface up to 10 m/s and in a borderline case at static air, the drying rate is low, even if the surface temperature is increased. The drying rates run to maximally 50 kg/m^2h. They are approximately comparable to the values depicted in fig. 2. With increasing air velocity the drying rate increases considerably. For example, the drying rate of g_D = 28 kg/m^2h attainable with free convection at the Toluene boiling point may be reached at the very low surface temperature of about 20° C at an average air velocity of about 60 m/s. It is, therefore, possible to keep the surface temperatures in desired limits, but nevertheless to considerably increase the drying rate by increasing the air velocity. Fig. 3, however, also shows that the slope of the drying rate is all the steeper, the higher the selected surface temperature.

The depicted relationships make it possible to compare drying systems with each other as to their efficiency. Drying systems which operate without a distinct air velocity, as for example the contact dryers, drying systems with

electro-magnetic waves, etc., are, despite a considerable temperature increase incapable of producing a high drying rate.

As by-product, which was created with the help of the compiled material data for Toluene required for the computation, we obtained an i-x-diagram for Toluene-air mixture (fig.4), which is useful for tracing and illustrating the drying processes of printing inks containing Toluene.

A high efficiency drying system is evidently only possible with greater air velocities. For this reason, the second part of this report will discuss partial results of individual studies which deal with the optimization of a high efficiency drying system, such as e.g. the impinging air jets - dryer.

To attain satisfactory optimization of an impinging air jet-dryer, a measurement of the local mass transfer coefficient taking into consideration various flow conditions and the geometric relationships is necessary. The mass transfer coefficient β is defined according to the following equation

$$\text{Drying rate} \ldots\ldots g_D = \frac{\beta}{R_D T} (P_{D_O} - P_{D_L}) \quad kg/m^2h \qquad (1)$$

We write

β = mass transfer coefficient m/h

R_D = gas constant of solvent vapor mkp/kg°K

T = average temperature in the boundary layer °K

P_{D_O} = partial pressure of the solvent vapor on the surface of the liquid kp/m^2

P_{D_L} = partial pressure of solvent vapor in the air kp/m^2

From the structure of equation (1) may be seen, that at a given temperature and partial pressure difference the mass transfer coefficient β determines the extent of the drying rate.

The measuring of the local mass transfer coefficient is in general, very difficult. The analogous magnitude, the heat transfer coefficient α is more easily determined by measuring techniques. Both magnitudes, based on the laws of similarity are distinctly related.

A heat-flow transducer which was mounted with its sensing surface flush with the surface of a plate, was used for measuring the local heat transfer

coefficient. Fig. 5 shows the heat-flow transducer which contains a heatable thin foil as a measuring element. A match is shown for comparison. Fig. 6 shows the entire test installation with the measuring devices used. The blower G in the foreground is connected with the nozzle casing DK via a diffuser DF. At the vent of the nozzle casing various tuyère bottoms in single or multiple jet arrangement may be fastened. Under the nozzle casing a plexiglass plate P, which is impinged by the air jets, is mounted on a solid stand and arranged to move in three directions x, y and z. This plate simulates the imprinted web. On the table in the center of the illustration we see the hot wire anemometer KTA which in principle is a Wheatstone Bridge which automatically rectifies itself. The heat-flow transducer is connected in a branch of the bridge and serves as a heat source and resistance thermometer simultaneously. The anemometer automatically keeps the temperature of the hot-foil constant, so that its heat loss under various flow conditions represents a measure for the local heat transfer coefficient.

The output voltage of the anemometer, which is required for the determination of the heat transfer coefficient, may be measured separately with the help of a five-digit digital voltmeter DV. For the turbulence measurements as well as for the correct adjustment of the transducer a cathode ray oscilloscope KO was used. With the help of an x-y recorder S, which may be seen on the right side of the illustration, the output voltage of the anemometer may be plotted by means of a displacement transducer as a profile. In the lower right hand half of the illustration, part of the nozzles used may be seen. These slot nozzles which were originally installed as calibration nozzles were, however, for comparison with multiple jet arrangements used also for the studies of air flow and heat transfer processes in single jet arrangements.

In the following, we will report exclusively on these tests. For certain reasons connected with the calibration of the transducer, the air jets had to be especially free of turbulence. These calibration nozzles have profiles which were calculated for an adiabatic expansion, whereby we assumed a constant pressure gradient along the jet axis. They fulfilled the condition of low turbulence very well. Two types were constructed: nozzle type 1 for compact installation in the bottom plate of the nozzle casing (height 20 mm) and nozzle

type 2 with a long outflow (height 200 mm). Both nozzle types are depicted in fig. 7. Fig. 8 again shows nozzle type 2 as installed in single impinging jet arrangement. The free jet expansion below a nozzle of 15 mm width (nozzle type 1) at a constant nozzle exit velocity of w_D = 48 m/s are shown by 3-dimensional drawing in fig. 9. The velocity profiles measured directly at the nozzle exit are very even both in x and y directions up to the exit. Such measurements were required, in order to determine the so-called core length of a free jet. By core length we mean the relationship between the distance z' and the nozzle width B, at which the maximum nozzle exit velocity is still retained in the jet axis. As a rule, the core length runs to $z'/B = 4$ to 5. The core length is primarily dependent on the intensity of turbulence of the free jet. The greater the intensity of turbulence at the nozzle exit, the smaller is the core length, because of heavy mingling with the ambient air.

Fig. 10 shows the dependency of the velocity w_{str} in the jet axis on the distance z' from the nozzle exit at various nozzle exit velocities w_D for nozzle type 1 in accordance with fig. 7. The core length of this jet is about $z'/B = 8$ and is obviously considerably larger than the core length found in actual practice.

The nozzle exit velocity is not directly a measure for that air velocity which directly influences drying. Rather the thickness-parallel velocity component in the boundary layer is responsible for the mass and heat transfer. This velocity component is dependent on maximum jet velocity prevalent at the center of the free jet at a distance z' corresponding to the nozzle-to-plate spacing Z. A great core length is, therefore, of special importance.

For measuring the heat transfer, the measuring arrangement shown in fig. 8 and 11 was selected. A segment of fig. 11 shows the compactly installed nozzle type 1 under the nozzle casing, a Pitot-tube SDS for measuring the nozzle exit velocity and a hot wire transducer HDS for measuring the turbulence. In fig. 12 may be seen plate P with the compactly installed heat-flow transducer WFG.

The plate is provided with insertable liners at various places, which may contain various heat-flow transducers as e.g. measuring connection for static pressure.

Although the local heat transfer coefficient at the stagnation point itself is not of great significance for the average heat transfer coefficient, the knowledge of its dependency on the nozzle-to-plate spacing Z and on the velocity w_D is desirable. Fig. 13 shows this for a nozzle (type 1) with an exit width B = 15 mm. Looking at the diagram the unusually high values for the heat transfer coefficient α strike us. The effective heat transfer coefficient is, as a matter of fact, smaller.

Thorough examinations have shown that at the stagnation point a fixed gauge factor $C_1 \approx 5.3$ is valid. We obtain the effective heat transfer coefficient α_{eff} by dividing the heat transfer coefficient $\alpha_{Gstr.}$ shown by the heat-flow transducer by C_1. The gauge factor is primarily dependent on the size of the hot-foil. Measurements taken of heat wires of smaller dimensions are known to behave similarly. If we plot the root value of the nozzle exit velocity on the abscissa - as in fig. 13, we find the measuring curves represented as straight lines. This means that the heat transfer coefficient is proportional to the 0.5 power of the nozzle exit velocity and thereby follows the mathematical interrelations for a laminary boundary layer. The following equation is thus valid

$$\alpha_{eff} = \alpha_{Gstr} \cdot \frac{K}{C_1} \cdot w_D^{0.5} \qquad (2)$$

Furthermore, the diagram shows that α_{eff} is likewise dependent on the nozzle-to-plate spacing without providing exhaustive information about this dependency. Fig. 14 deals specially with this dependency. We see that at a given velocity two maxima occur for the local heat transfer coefficient. (in the selected example - at about Z/B = 0.5 and Z/B = 21). Which of the two maxima is the higher depends on the intensity of turbulence of the jet flow. If there is low turbulence, then the second maximum is the higher. If, however, there is a very turbulent flow, the first maximum is higher. The second maximum is approximately retained, since the decline of the heat transfer coefficient is compensated for by the higher turbulence as a result of the shortened core length. As shown from measurements taken by others, e.g. Gardon and Akfirat [5], the second maximum, however, shifts to lower values of Z/B. These relationships also point to the great importance of a low turbulence jet with great core length.

The first maximum may not be used in a printing press because of the small distance between nozzle exit and material to be imprinted. The second maximum should occur at as high a Z-value as possible, so that a high operational safety of the press is achieved. This further underlines the significance of the core length.

Of special interest, of course, are the local heat transfer coefficients along the surface (in x-direction). Fig. 15 shows measuring results for both nozzle types.

Hereby the nozzle exit velocity for all measurements was $w_D \approx 48.6$ m/s. The heat transfer coefficient $\alpha_{G\,str}$ measured by the heat-flow transducer is plotted on the ordinate. In order to get the values of the effective heat transfer coefficient α_{eff}, the $\alpha_{G\,str}$-values again have to be divided by a gauge factor. Whether this gauge factor along the whole plate length corresponds to the gauge factor C_1 determined from the calibration at the stagnation point or whether with very great plate length another gauge factor based on the turbulence flow has to be used, is still subject of further investigations. The distance from the stagnation point x was in each case made dimensionless with the nozzle width B, in order to better be able to compare the curves with each other.

In observing these curves, we first notice that the local heat transfer coefficients above the dimensionless stagnation point distance x/B show great fluctuations. The curves show maxima at two points. Smaller nozzle widths yield altogether higher heat transfer coefficients at approximately the same Z/B values.

All curves show a minim heat transfer coefficient in the examined range of Z/B at the stagnation point. Thanks to the small size of the hot-foil in flow direction (foil width 0.2 mm) we may speak of a local measurement even at smallest nozzle widths. With earlier measurement methods, the active measuring width of the transducer used, was mostly of the magnitude of the nozzle width, so that in all probability the minimum at the stagnation point could not be determined. Earlier measurements all show a maximum for the heat transfer coefficient (Gardon and Akfirat [5]). We would like to note here without reproducing the measuring results, that with an increase in the

distance Z, the minimum at the stagnation point increases more and more until it finally does become a maximum.

A fundamental difference between the course of curves 1 and 2 and thereby between both nozzle types cannot be established. This, however, means, that a compactly installed nozzle (type 1) may be utilized as a single jet just as well as type 2. Because of its small height it offers the additional advantage of space economy in design. In multiple jet arrangements the nozzle of type 2 is, however, used to advantage, since for the carrying off of air, the space between the jet contours is very beneficial.

Summary:

With the help of known theoretical formulations for the evaporation process of liquids, the influence of temperature and of air velocity on the drying rate with Toluene evaporation as an example, was determined. A fundamental evaluation of various drying systems is thus possible. As by-product in the computations an i-x diagram for a Toluene-air mixture was created.

With regard to the optimization of efficient air circulating drying systems, we showed by means of local heat transfer measurements, how the change of air velocity, of the nozzle width and of the nozzle-to-plate spacing, affects the heat transfer coefficient and thus the mass transfer coefficient determining the drying rate.

The results represented do not answer all the questions, but do show distinctly that until now too little attention was paid to the nozzle design.

References:

1. Schrader H.: Trocknung feuchter Oberflächen mittels Warmluftstrahlen. Strömungsvorgänge und Stoffübertragung. VDI-Forschungsheft 484 (1961)

2. Schlünder E.U. und Gnielinski V.: Wärme- und Stoffübertragung zwischen Gut und aufprallendem Düsenstrahl. Chem.-Ing.-Techn. Heft 9/10 (1967) S. 578/584

3. Petzold K.: Der Wärmeübergang an einer senkrecht angeströmten Platte. Wiss.Z. Techn.Univ. Dresden 13 (1963) 4.4, S.1157/1161

4. Perry K.P.: Heat Transfer by Convection from a Hot Gas Jet to a Plane Surface. Prog. Inst. Mech. Eng. Vol. 168 (1954) S. 775/780

5. Gardon R. and Akfirat C.: The Role of Turbulence in Determining the Heat-Transfer Characteristics of Impinging Jets. Int. J. Heat Mass Transf. Vol. 8 (1965), S. 1261-1272

Oberflächentemperaturen t_W einer flüssigen Toluolschicht bei verschiedenen Lufttemperaturen t_L und verschiedenen Dampfteildrücken P_{D_L} unter Berücksichtigung der veränderlichen Stoffwerte für Toluol–Luft–Gemisch und unter der Annahme einer logarithmischen Verteilung in der Diffusions–Schicht für Temperatur und Dampfteildruck.

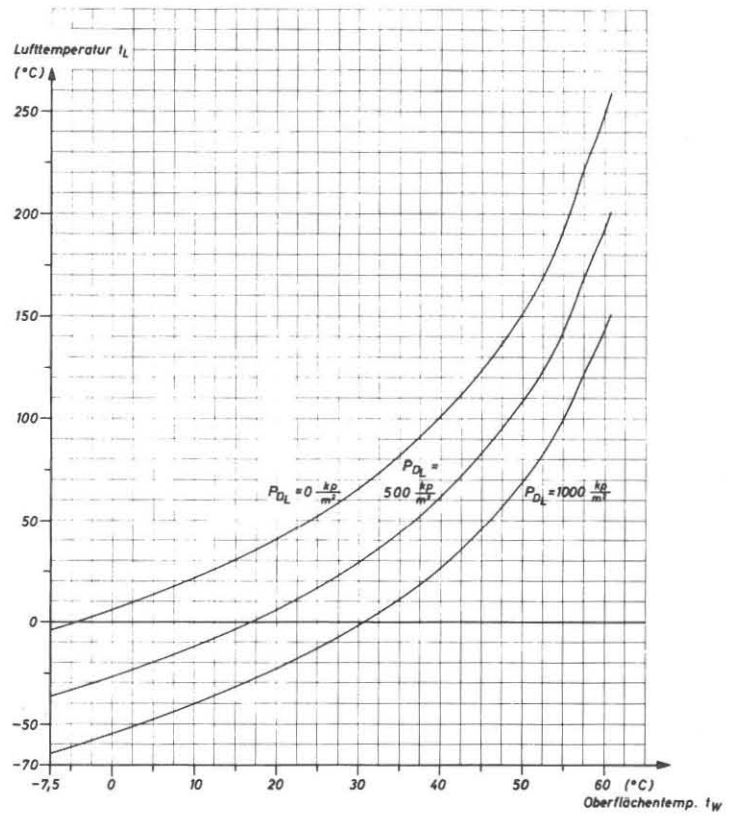

Fig. 1: Surface temperatures t_W of a liquid Toluene layer at various air temperatures t_L and various vapor partial pressures P_{D_L} taking into consideration the variable material data for Toluene–air mixture and by assuming a logarithmic distribution in the diffusion layer for temperature and vapor partial pressure.

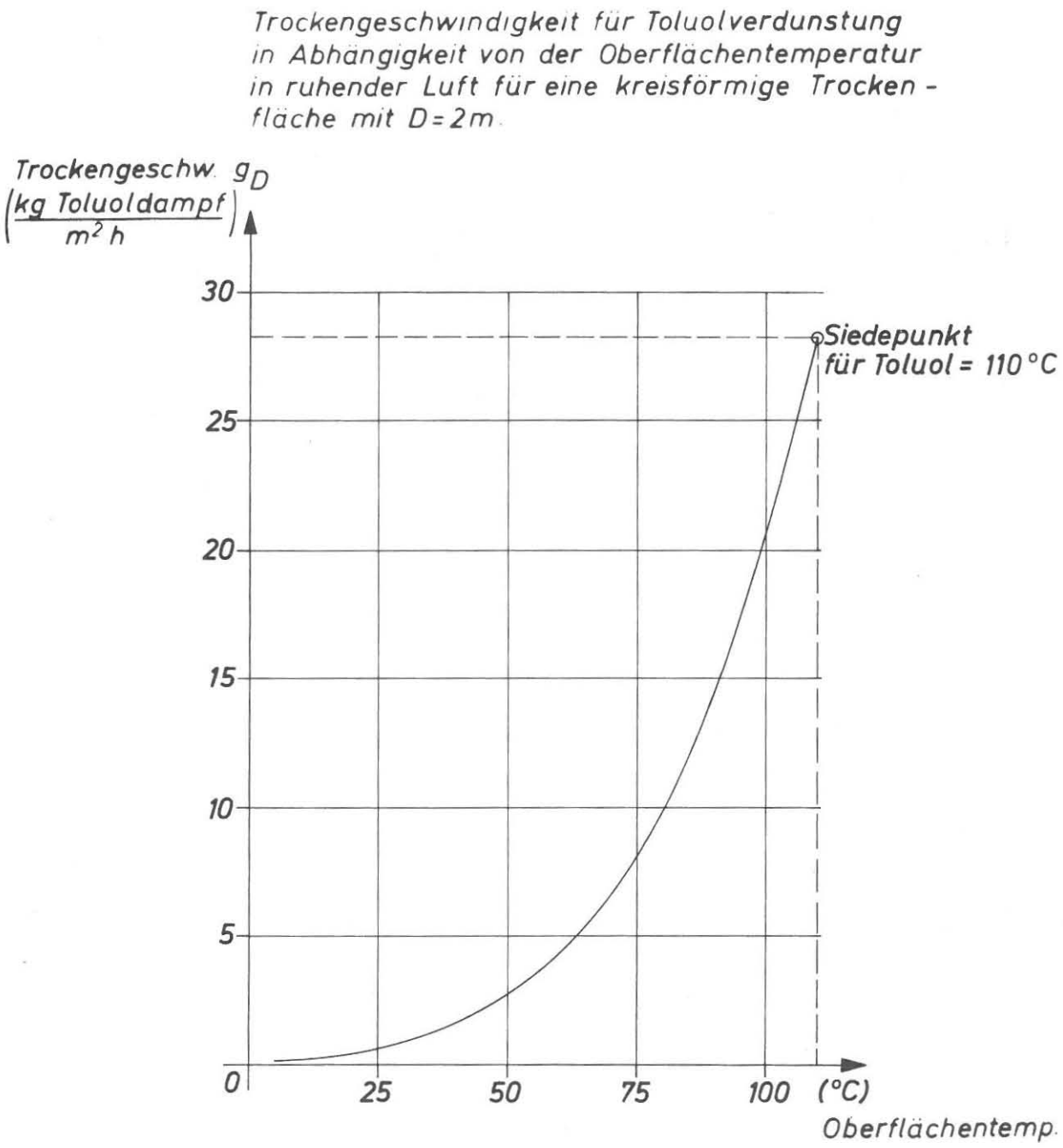

Fig. 2: Drying rate for Toluene evaporation in dependency on the surface temperature in static air for a circular drying area with D = 2 m.

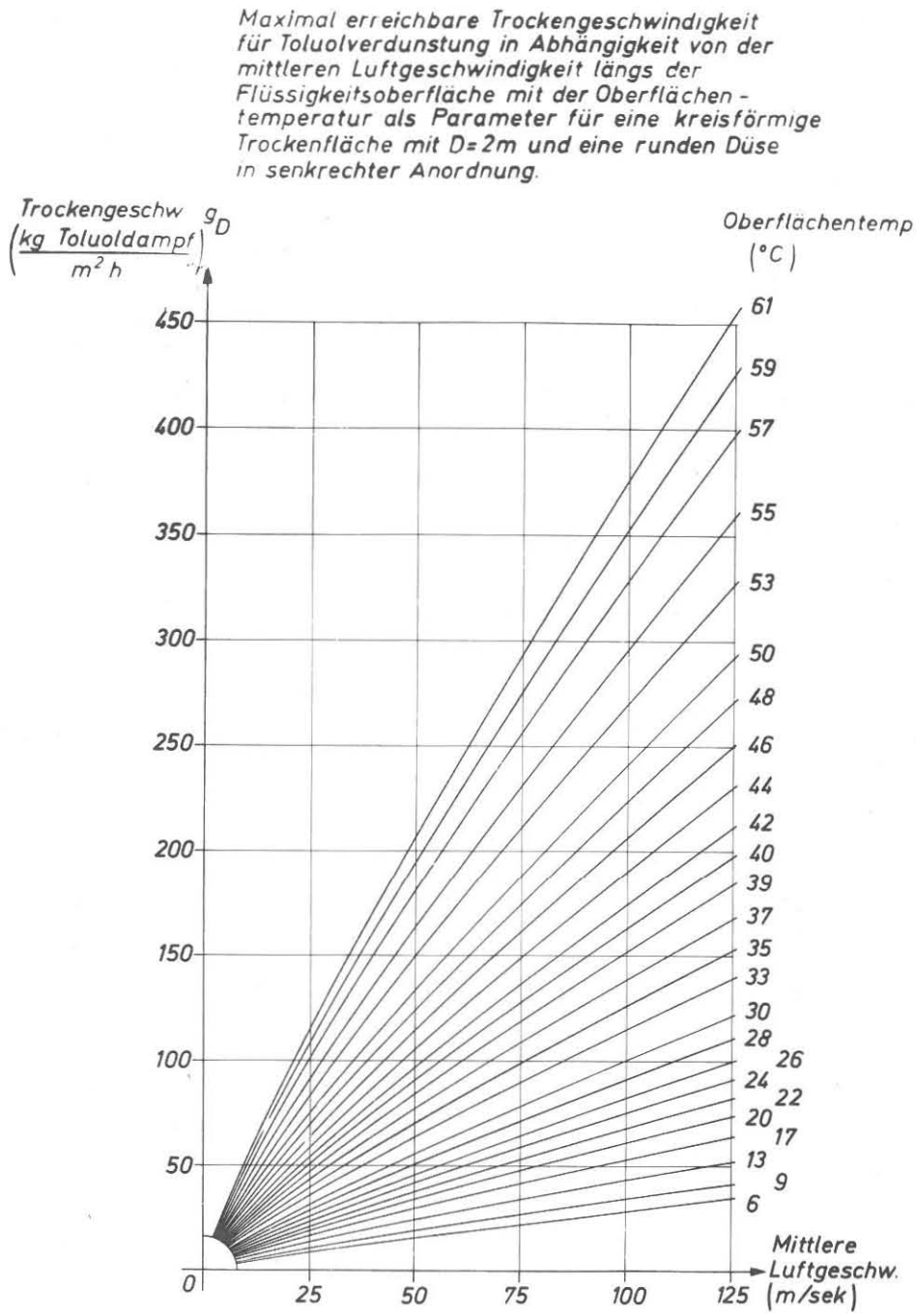

Fig. 3: Maximum attainable drying rate for Toluene evaporation in dependency on the average air velocity along the liquid surface with the surface temperature t_w as a parameter for a circular drying area with D = 2 m and a single circular impinging jet arrangement.

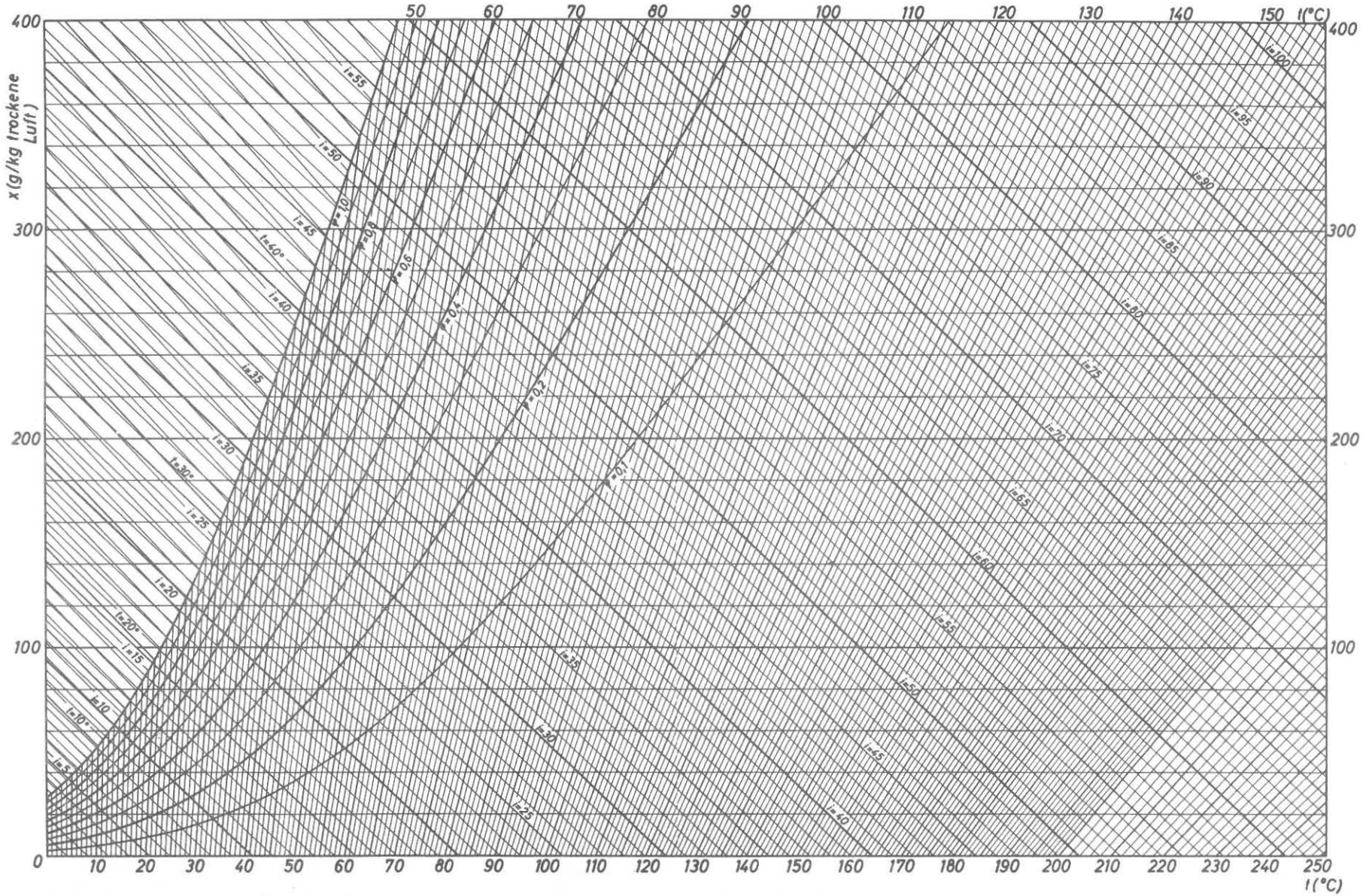

Fig. 4: i-x diagram for Toluene-air mixture in the range 0° C - 250° C and P = 760 torr

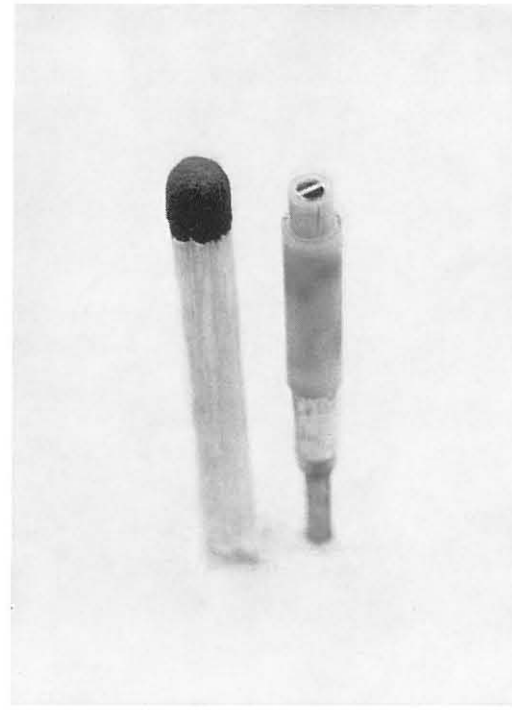

Fig. 5: Heat-flow transducer for measuring local heat transfer coefficient.

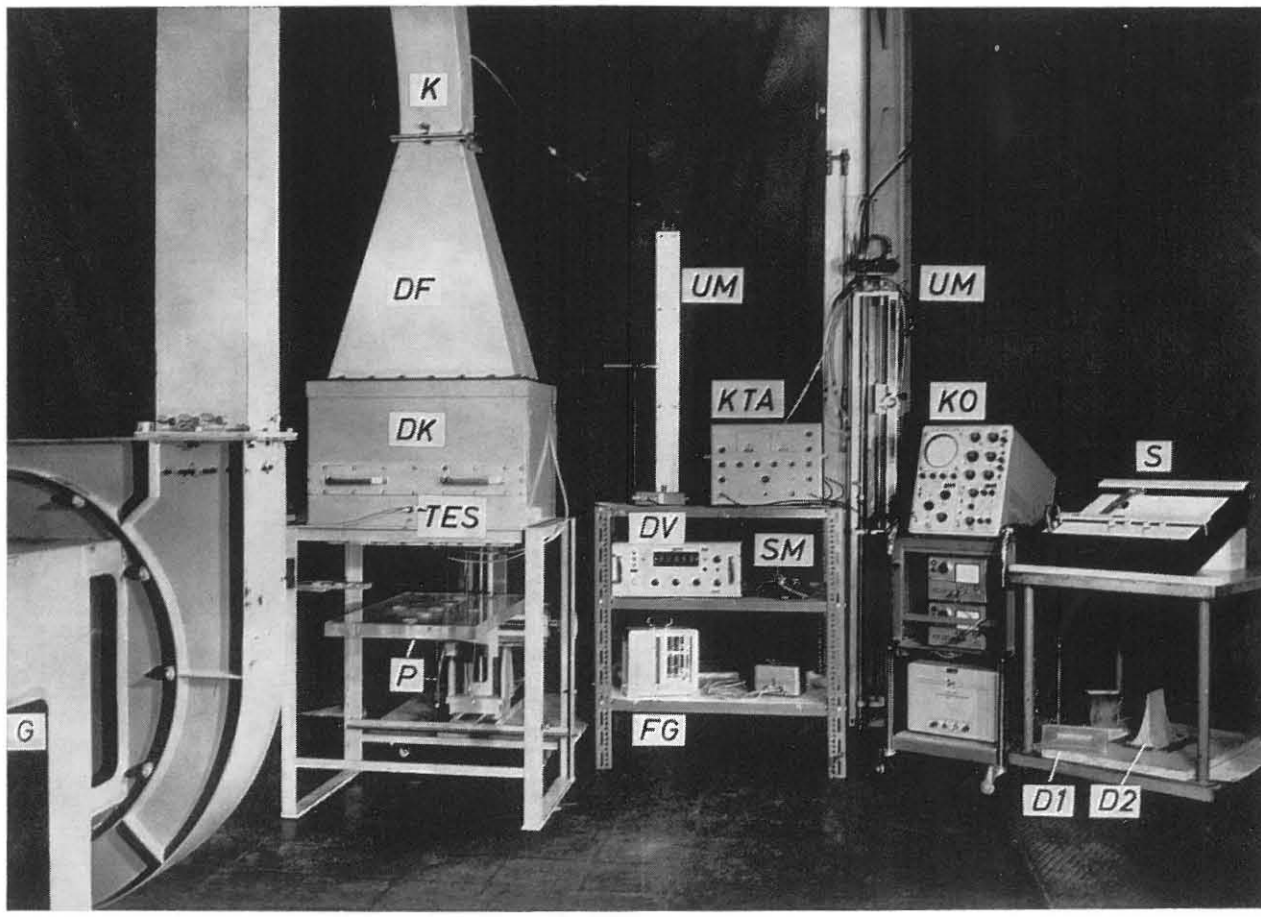

Fig 6: Test equipment and measuring devices: G: Blower; DK: nozzle casing; DF: diffuser; P: plexiglass plate; KTA: constant temperature-hot-wire anemometer; DV: digital voltmeter; KO: cathode ray oscilloscope; S: x-y recoder; D 1: nozzle type 1; D 2: nozzle type 2; UM: tube manometer; SM: inclined tube manometer; FG: air moisture measuring device; TES: Thermocouple in nozzle casing.

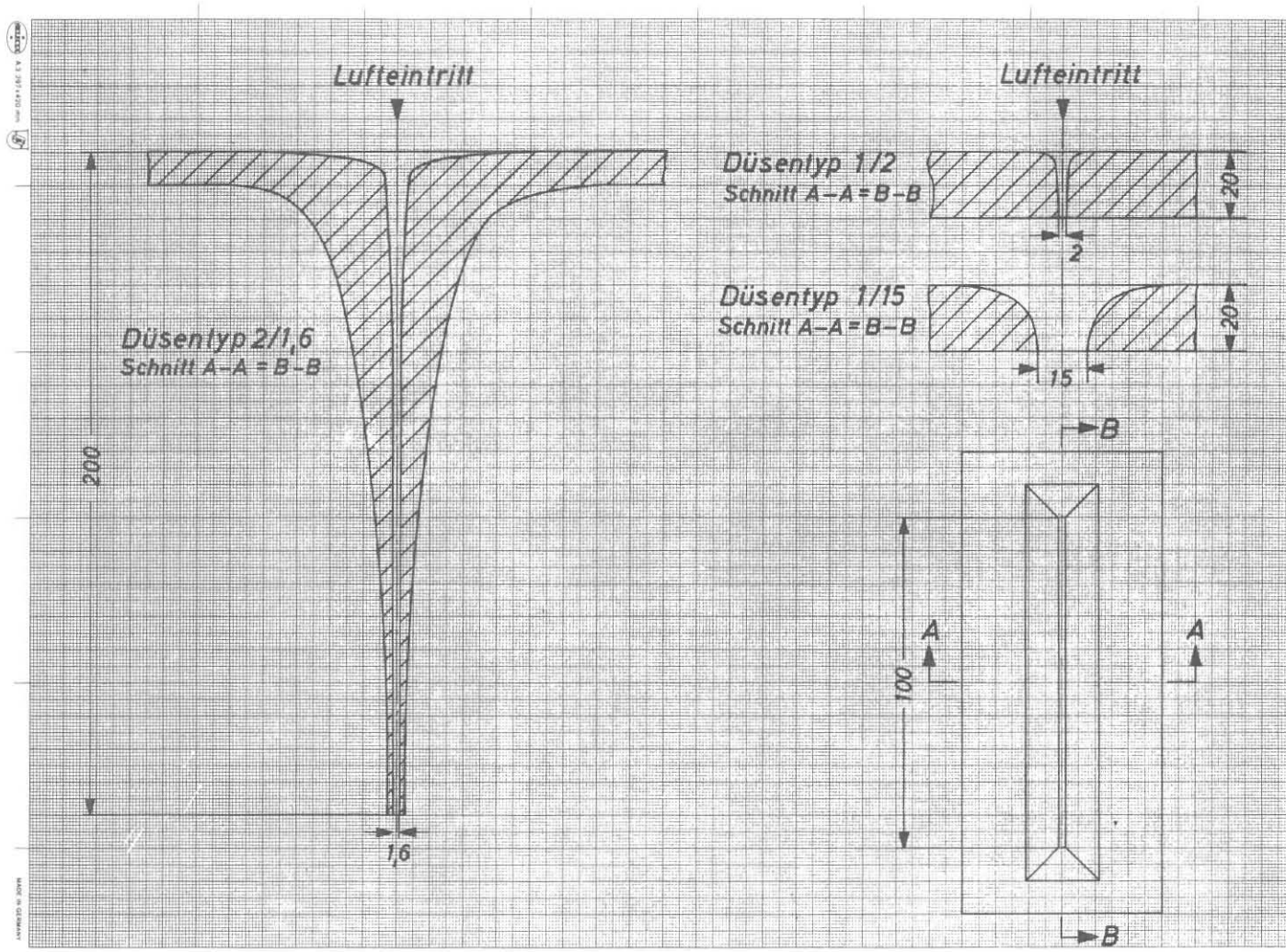

Fig. 7: Various nozzle types (Nozzle exit length L for all nozzles L=100 mm).

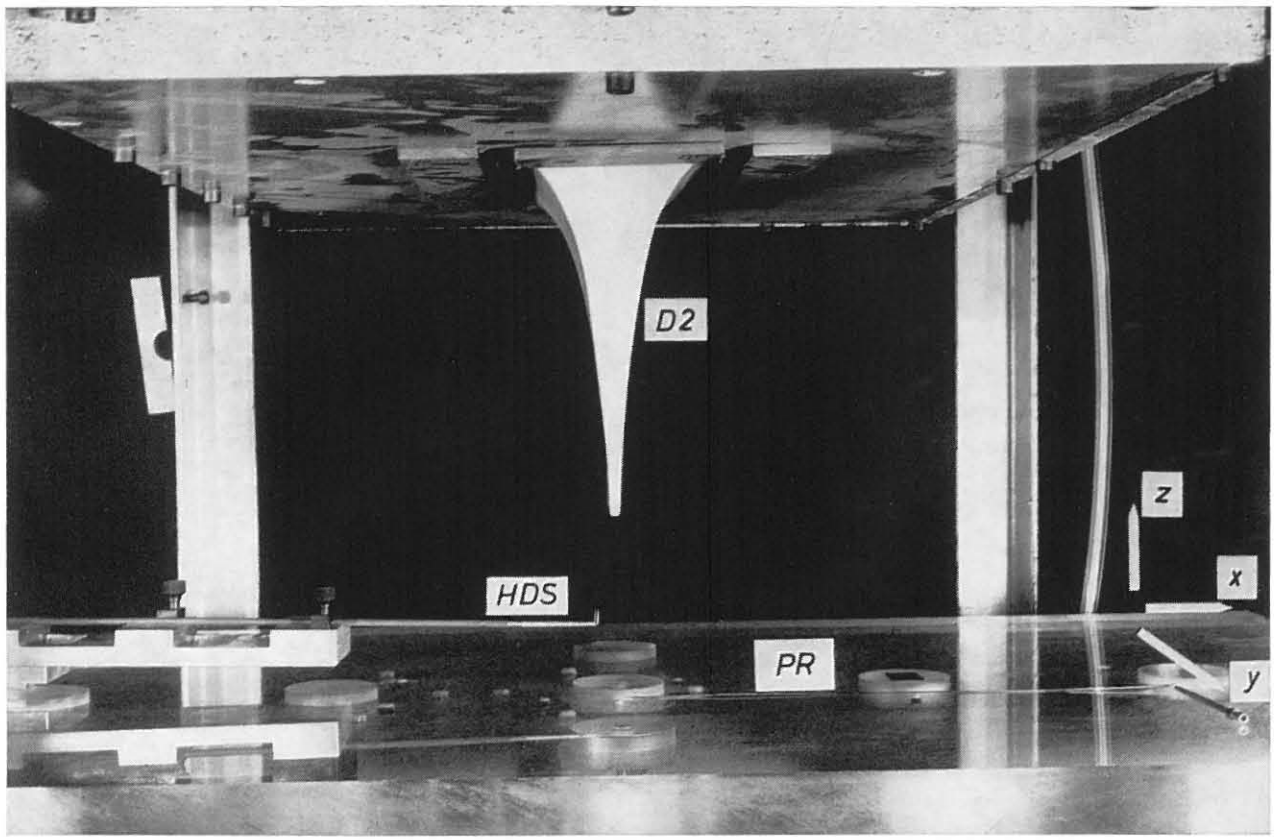

Fig. 8: Nozzle type 2 as single impinging jet arrangement. HDS: hot-wire transducer; PR: Pitot-tube.

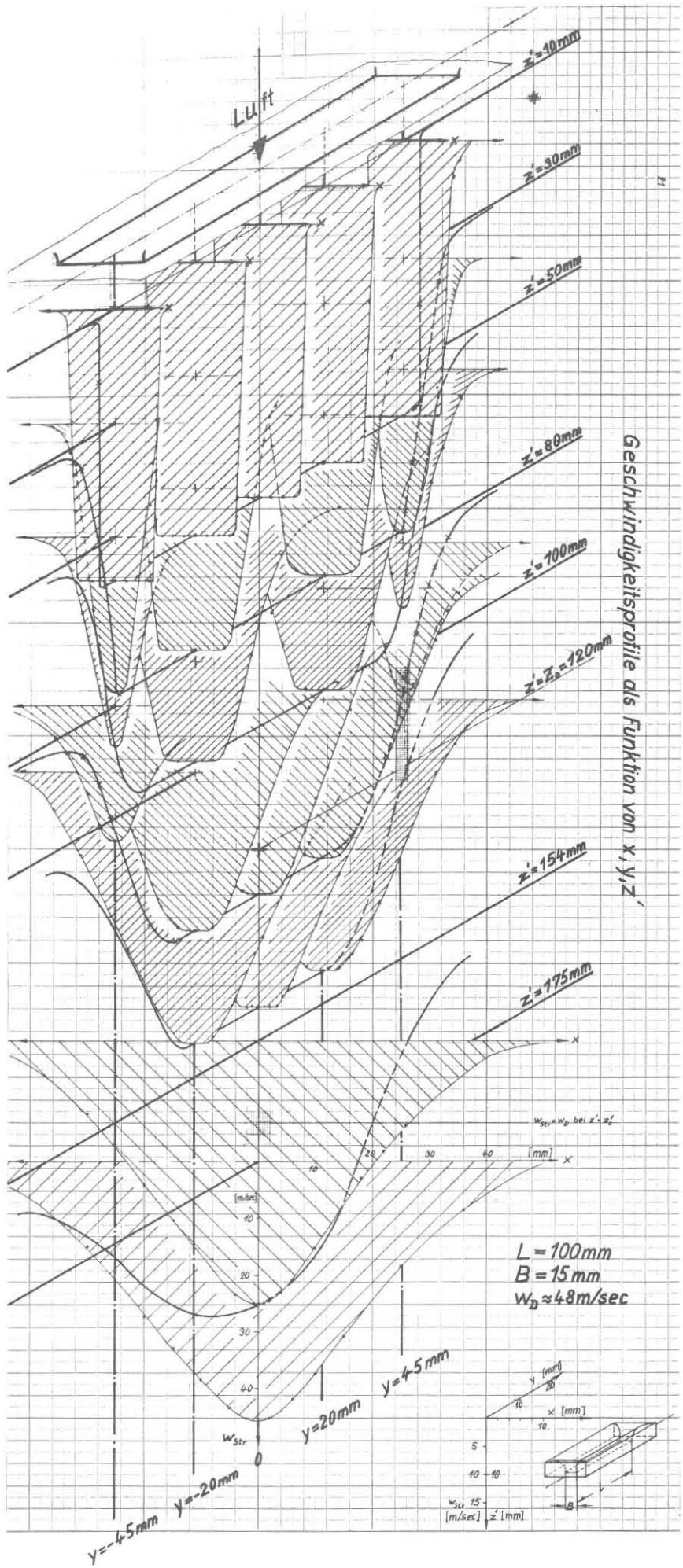

Fig. 9: Velocity profile under an air jet (type 1) in three-dimensional drawing for a nozzle exit velocity w_D = 48 m/s.

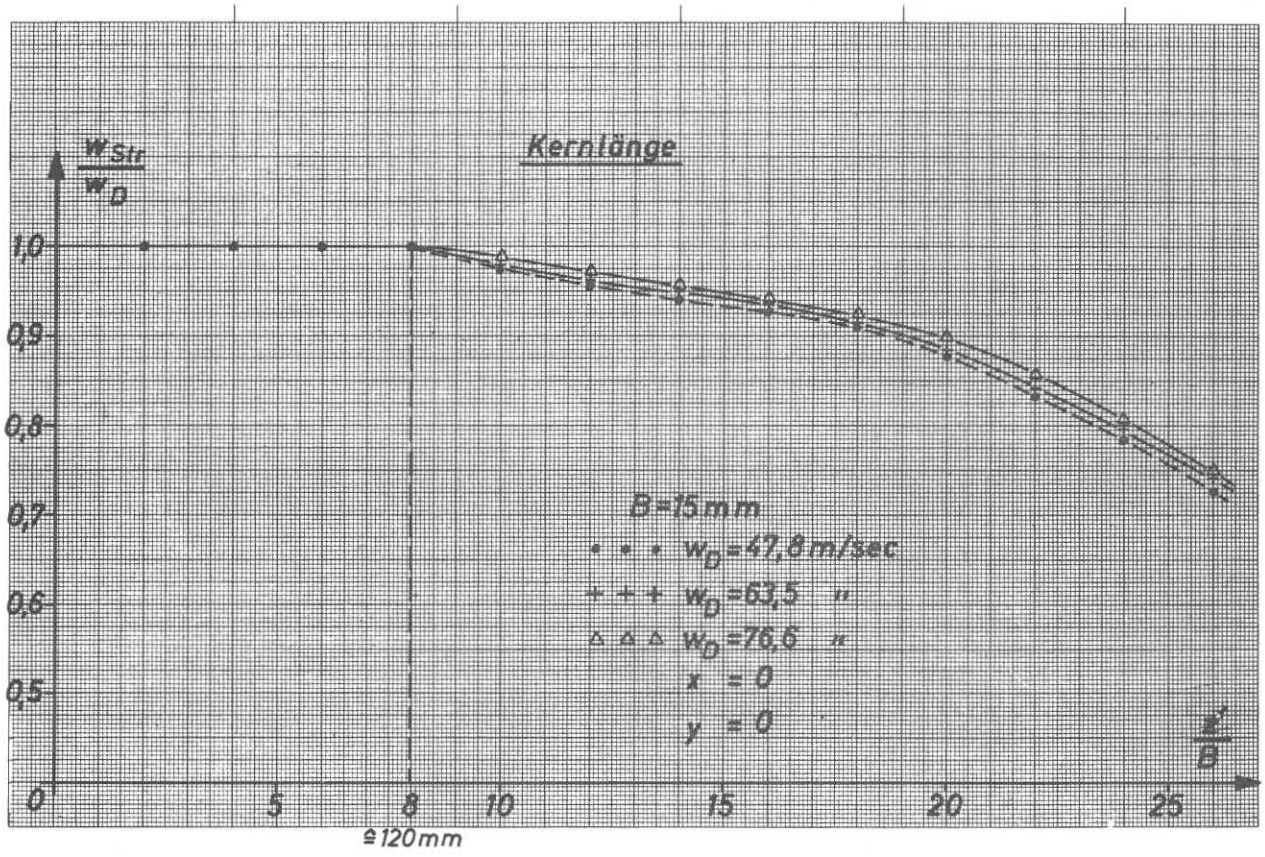

Fig. 10: Core length of an air jet (nozzle type 1, nozzle width B = 15 mm) in jet axis z′ at various nozzle exit velocities.

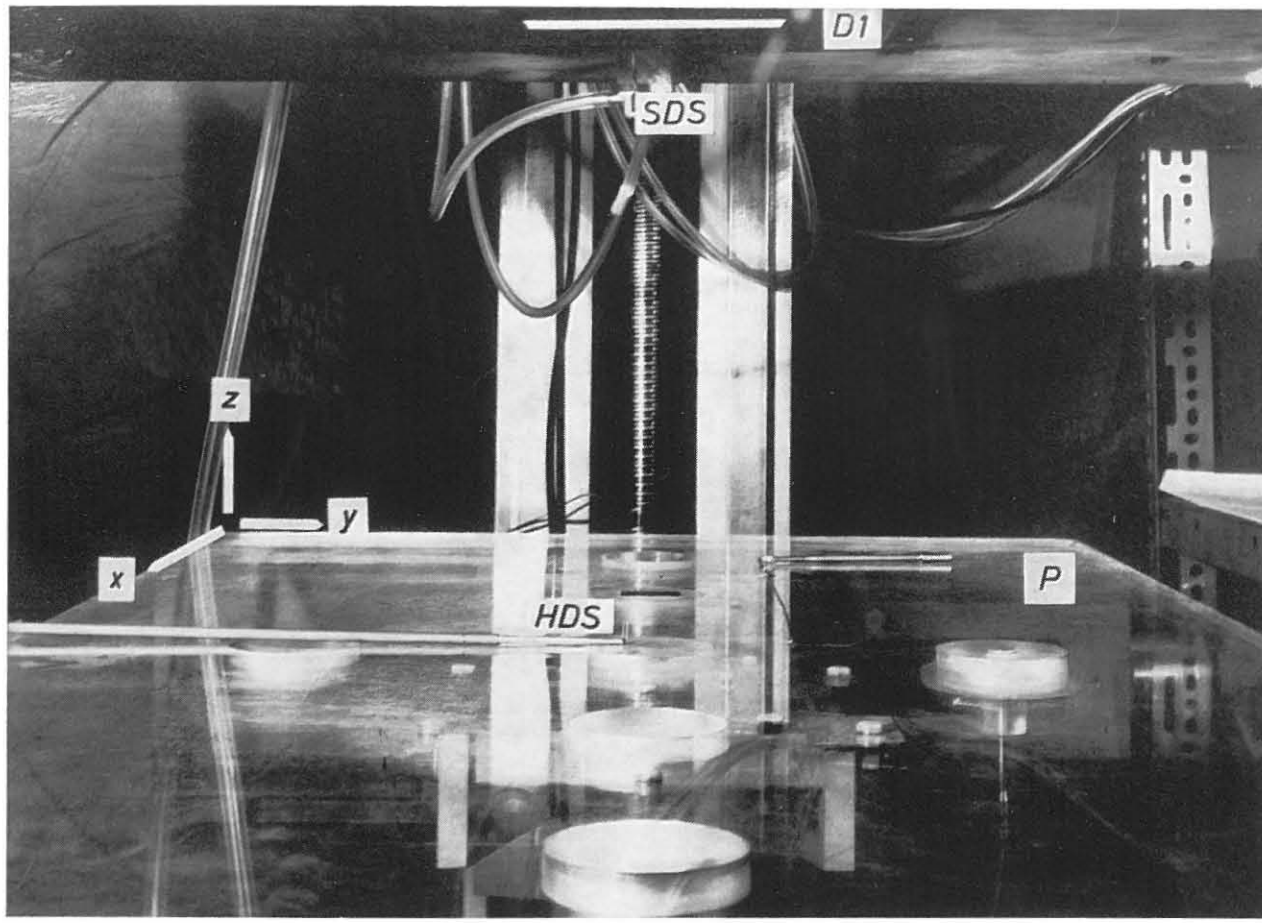

Fig. 11: Nozzle type 1 as single impinging jet arrangement. SDS: Pitot-tube; HDS: hot-wire transducer.

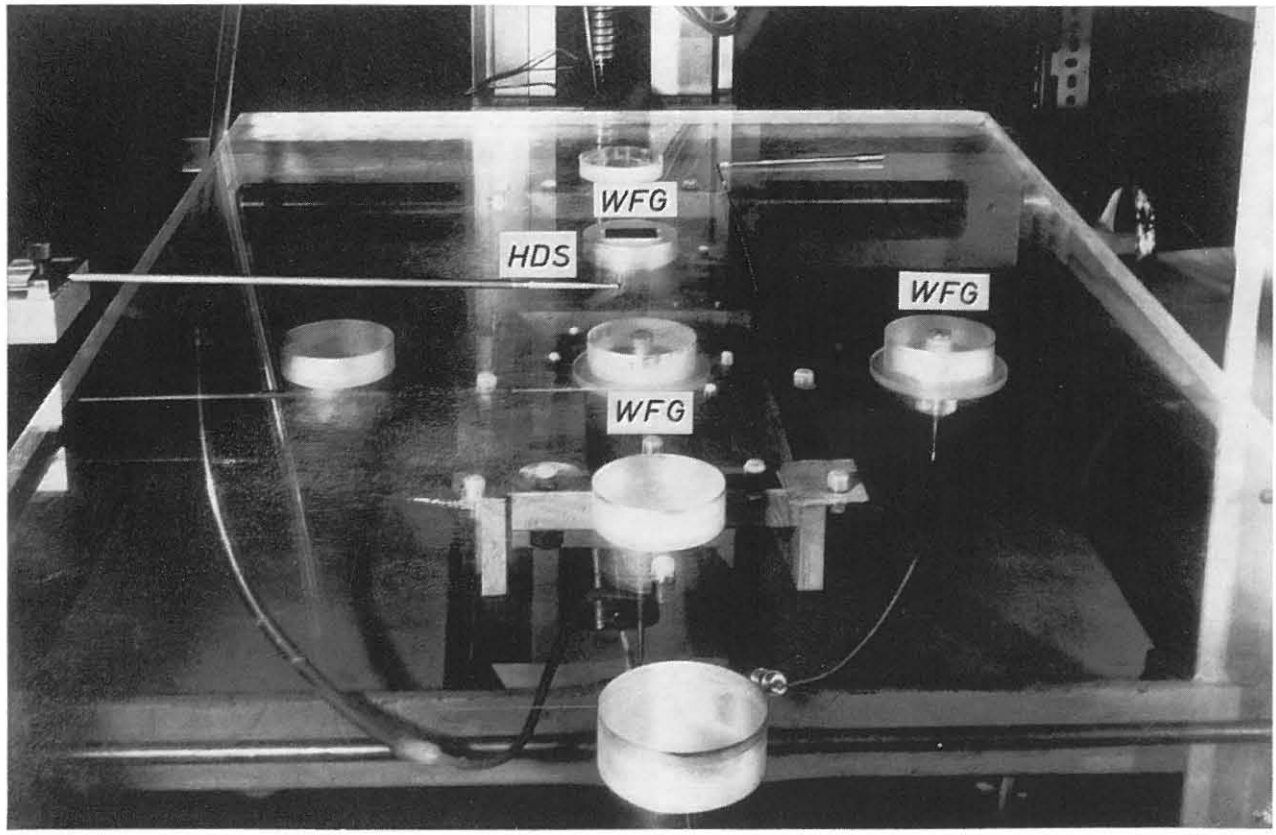

Fig. 12: Plate P hit by vertical flow with built-in heat-flow transducer WFG.

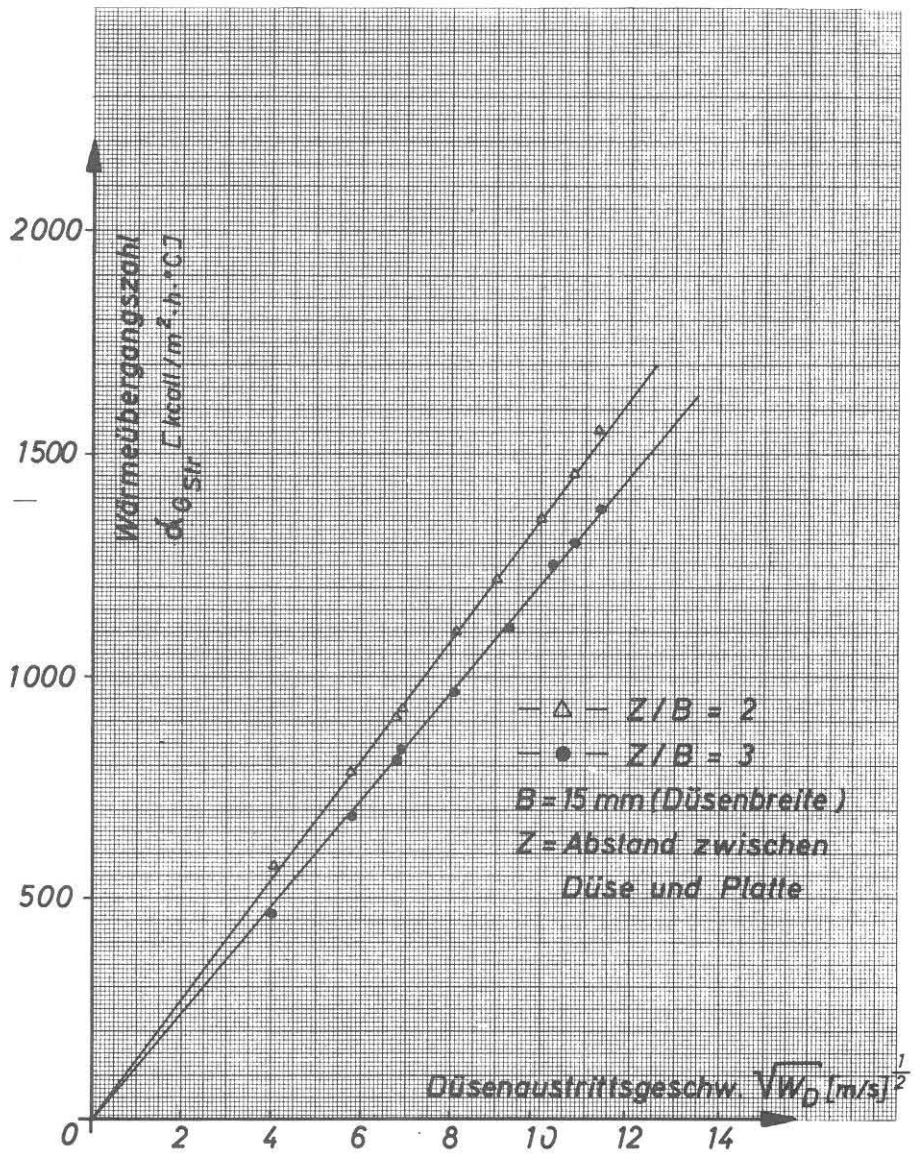

Fig. 13: Dependency of the heat transfer coefficient α_{eff} measured at stagnation point on the nozzle exit velocity for various nozzle-to-plate spacings

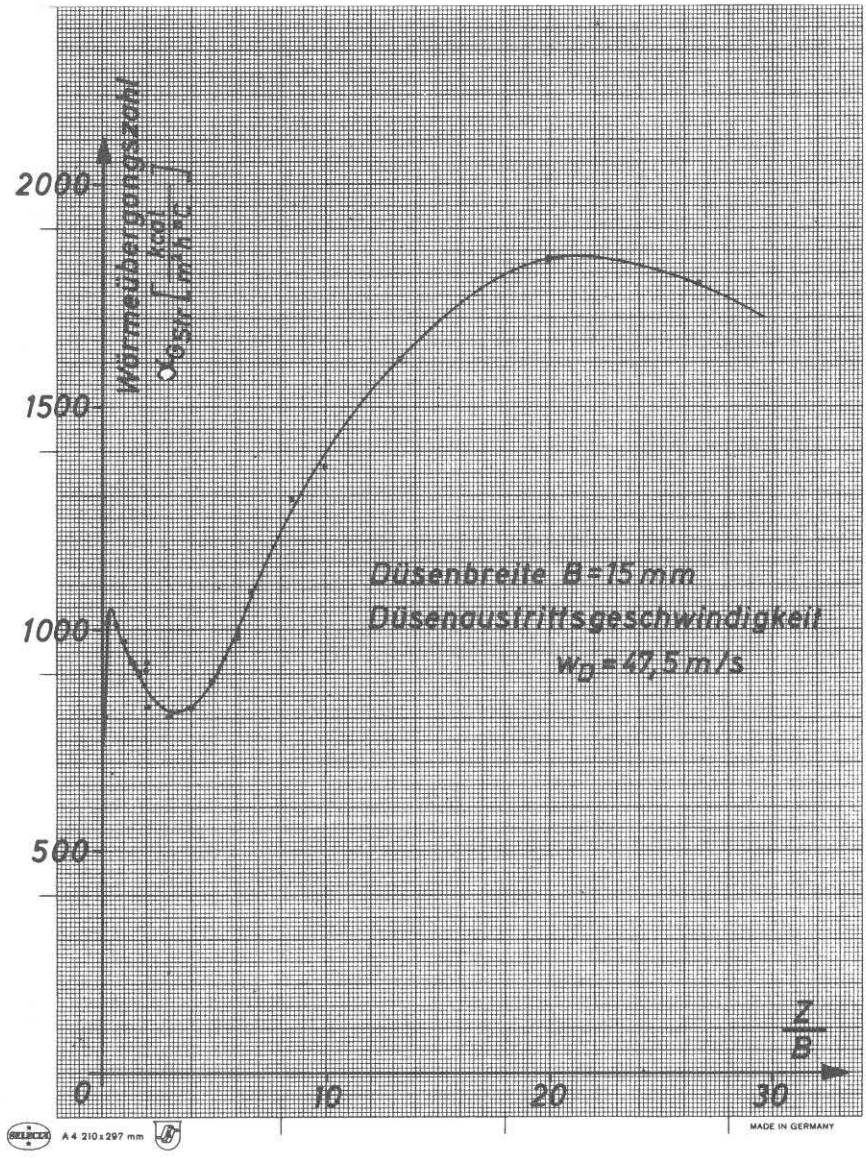

Fig. 14: Dependency of the heat transfer coefficient α_{Gstr} measured at stagnation point on the dimensionless nozzle-to-plate spacing Z/B at a constant nozzle exit velocity.

Verlauf der gemessenen örtlichen Wärmeübergangszahl α_{Gstr} in Abhängigkeit von dem dimensionslosen Staupunktabstand X/B unter verschiedenen Schlitzdüsen bei einer konstanten Düsenaustrittsgeschwindigkeit von $w_D \approx 48{,}6$ m/sec

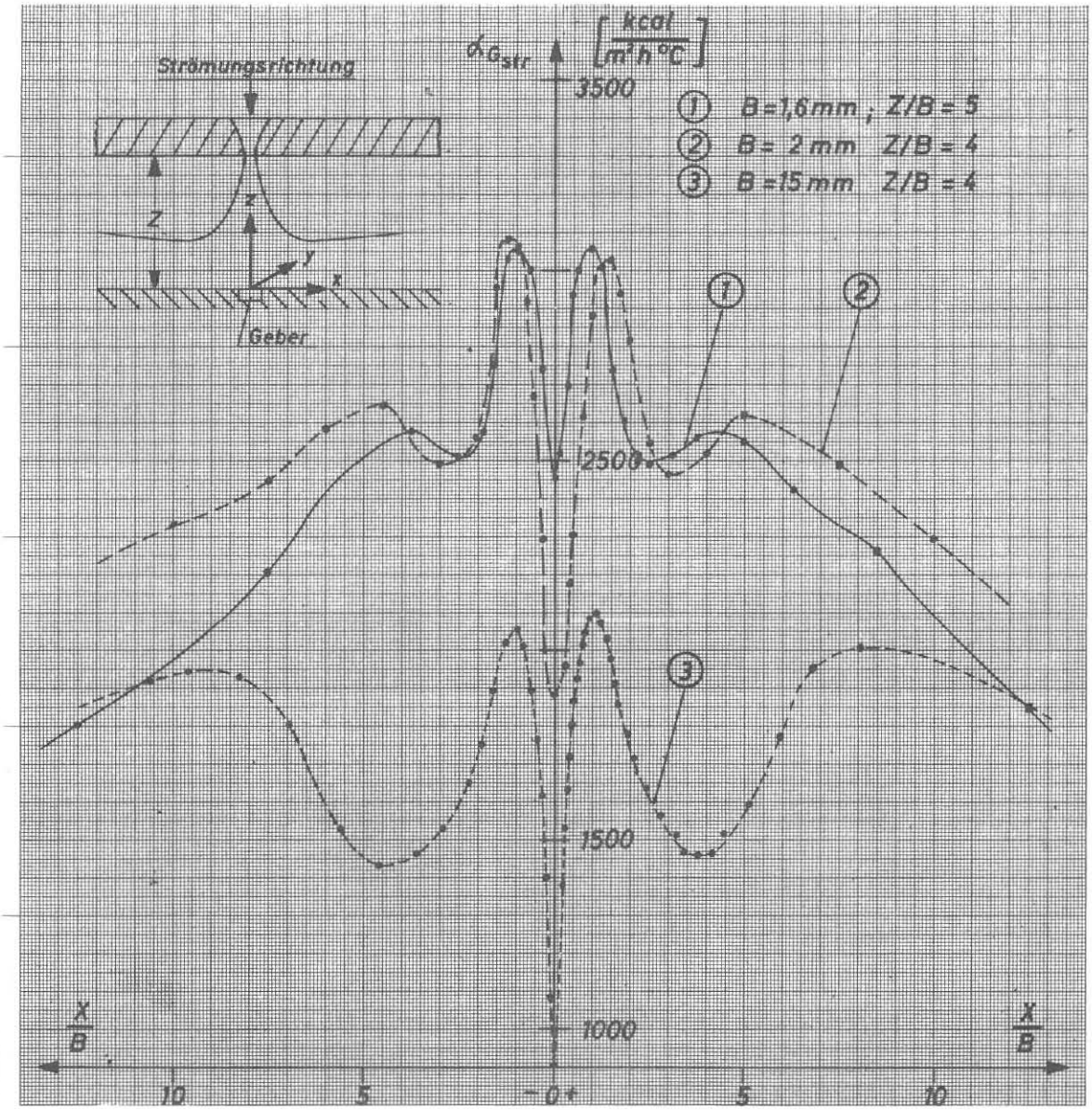

Fig. 15: Locally measured heat transfer coefficient α_{Gstr} in dependency on the dimensionless stagnation point distance X/B under various nozzles at a constant nozzle exit velocity of w_D = 48.6 m/s. Curve 1: nozzle type 2, curves 2 and 3: nozzle type 1.